Creating Data-Driven Turbulence Models Using PIV

Steven J. Beresh,* Nathan E. Miller, Eric J. Parish, Matthew F. Barone, and Jaideep Ray

Sandia National Laboratories, Albuquerque, NM, 87185, USA
*: Corresponding author: P.O. Box 5800, Mailstop 0825, (505) 844-4618, email: sjberes@sandia.gov

Keywords: PIV, Data Assimilation

ABSTRACT

Data-driven turbulence models have been created for a k-ε RANS model based on PIV data in a jet in crossflow. In the simpler of two implementations, the nominal value of the model coefficient C_μ was replaced with an optimized value calibrated to the PIV results. Despite being based on only four flow cases of a canonical configuration, the optimized model demonstrated superior performance over 48 flow cases of increasing complexity. A second, more sophisticated data-driven model has been created by mapping a spatially variable C_μ to flow state variables using machine learning of experimentally measured flow field properties of the turbulence. This second model has been implemented in a production RANS code but requires further improvements before it can return results deviating from either the nominal or calibrated C_μ models.

1. Introduction

Most practical Computational Fluid Dynamics (CFD) simulations continue to rely on Reynolds-Averaged Navier Stokes (RANS) approaches, including the jet interaction applications upon which the present effort is focused. Although Large Eddy Simulation (LES) and Direct Numerical Simulation (DNS) produce greatly superior results in terms of accuracy (e.g., [1]), RANS remains the predominant means of providing engineering predictions for the simple reason that it is much less computationally expensive. For engineering campaigns that may require simulation of scores or even hundreds of cases, no alternative to RANS is presently feasible. Even as hybrid RANS/LES methods mature, turbulence closure models remain an inherent component of the simulation.

One of the most utilized RANS turbulence models is the k-ε model, which introduces coupled conservation equations for the turbulent kinetic energy (k) and the dissipation rate (ε) of that energy [2, 3]. This model then uses the turbulent-viscosity hypothesis to approximate the unresolved Reynolds stresses ($\overline{u_i'u_j'}$) using the mean rate-of-strain tensor via the Boussinesq approximation. This typically takes a linear form as

$$2\nu_t\overline{S_{ij}} = -\overline{u'_i u'_j} + \frac{2}{3}k\delta_{ij} \quad (1)$$

where the overbars represent Reynolds averages, ν_t is the scalar eddy viscosity, $S_{ij} = \frac{1}{2}\left(\frac{\partial U_i}{\partial x_j} + \frac{\partial U_j}{\partial i}\right)$ is the mean rate-of-strain tensor, and δ_{ij} is the Kronecker delta, though non-linear models have also been proposed and used (e.g., [4]). One of the primary parameters in any *k*-based RANS model, including *k*-ε, is the model coefficient C_μ, which is used to define the eddy viscosity based on *k* and ε as

$$\nu_t = \frac{C_\mu k^2}{\varepsilon} \tag{2}$$

This relationship is a key link between the evolution of the turbulent kinetic energy and the conservation equations for momentum and energy, and thus the specification of C_μ is pivotal in the fidelity and robustness of any RANS simulation. The value of C_μ and the other coefficients of the *k*-ε model ordinarily are presumed to be universal for a wide variety of canonical flows.

It may be recognized that all the terms to determine the eddy viscosity in Eqs. (1) and (2) are, in principle, accessible via modern PIV technology, and in fact eddy viscosity has been measured experimentally [5-8]. The dissipation rate, ε, is more challenging to estimate given that it occurs at small scales that may lie below the spatial resolution of PIV, but nonetheless several methods have successfully estimated values of ε (e.g., [9-12]). Therefore, a well-crafted PIV experiment can measure the properties that underlie turbulence models for at least a portion of the flow field, and thereby produce means of adjusting the value of C_μ or other modeling parameters to potentially improve performance in a selection of flows.

Meanwhile, the advancement of PIV capability, especially volumetric measurements, has leveraged fluid dynamics governing equations and numerical methods at the heart of CFD, an approach typically labelled as data assimilation. The rich data fidelity of time-resolved PIV in concert with volumetric methods, usually Lagrangian Particle Tracking (LPT), provides higher-fidelity velocity fields determined using fits to governing equations such that the results must reflect what is physically permitted. Moreover, the pressure field is determined through solution of the momentum equation as an inherent part of solving for the flow field that best fits the measured velocity data. Such methods were initiated from the seminal vortex-in-cell (VIC) technique based on a vorticity transport equation [13], expanded to include minimizing material derivative disparities in VIC+ [14] or additional continuity constraints in VIC# [15]. The related code FlowFit, tailored to LPT volumetric methods, minimizes incompressible velocity field divergence in both space and time to obtain reconstructions of the velocity and pressure fields onto regular grids [16, 17].

These data assimilation methods as applied to PIV greatly boost the fidelity of the information returned, but they suffer from a fundamental restriction: they apply only to the test case measured. They cannot return data predictive of the flow as governing parameters or geometries are altered. In contrast, RANS models offer a generalized predictive capability for a class of flows – but they suffer from the well-known

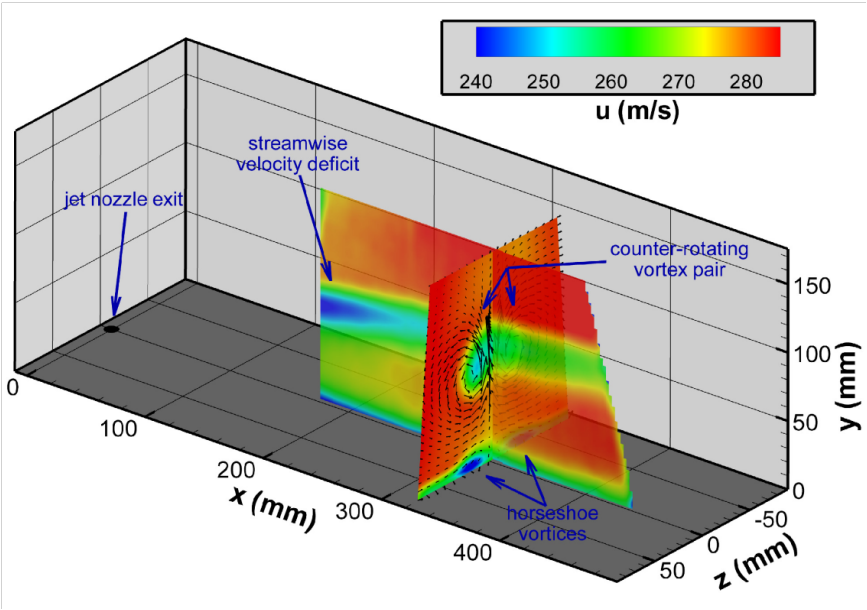

Fig. 1 Mean streamwise velocity data collected via PIV downstream of the jet nozzle from the experimental campaigns described in Beresh *et al* [20, 21]. Previously published in Ray *et al* [24].

accuracy limitations inherent in turbulence closure models.

Can the performance of RANS models be improved through use of PIV for determination of the turbulence model parameters based on the real physics of an experiment? The present insights suggest that PIV data may be used to determine the eddy viscosity and the dissipation rate and thus also C_μ. This maintains the architecture of existing RANS closure models, thereby expanding their functionality to data-driven models without necessitating creation of a new computational structure. With C_μ calculated directly from relevant experimental data, RANS models developed on simpler canonical flows may be adapted to offer improved predictive accuracy on a targeted class of flows.

2. Previous PIV Experiments

The PIV data are of a jet-in-crossflow configuration which has been studied and reported on for many years [18-21] and is depicted in Fig. 1. The reader is referred to the cited works for finer details on the experiments while only a brief synopsis is presented here.

Experiments were conducted in a Mach 0.8 flow through the 305 × 305 mm test section of Sandia National Laboratories' Trisonic Wind Tunnel (TWT). A supersonic jet was exhausted transversely into the flow from a Mach 3.73 nozzle positioned upstream of the region from which data were collected and mounted into one wall of the tunnel's test section. The conical nozzle was designed with an expansion half-angle of 15° with an exit diameter of 9.53 mm. The ratio of the dynamic pressure of the jet to that of the freestream

was nominally J = 10.2 but varied as a test parameter. The freestream Reynolds number based on the jet exit diameter was 2×10^5.

Stereoscopic PIV data were collected on two orthogonal planes downstream of the jet nozzle. The first plane was the wall-normal *x*-*y* plane oriented along the jet centerline ($z = 0$), perpendicular to the wall. The second plane was a *y*-*z* plane oriented orthogonally to the freestream, positioned downwind of the nozzle at $x = 219$ mm in one experiment and $x = 321$ mm in another.

The PIV data were processed using LaVision's DaVis v8.4. A total of 1500 vector fields were acquired for the *x*-*y* plane, while 9600 independent fields were used for the *y*-*z* plane. Optimal PIV image interrogation techniques were necessary to determine eddy viscosity and dissipation rates with sufficient precision, which are detailed in Beresh *et al* [22] and Miller and Beresh [23].

3. Calibrated RANS Model

Due to the complex flow topology of a turbulent jet in crossflow, RANS models built upon simpler canonical flows have struggled to quantitatively reproduce experimental measurements of the richer physics of the jet in crossflow. The most straightforward approach to incorporating PIV data into a RANS model is to recast the value of C_μ from its nominal value of 0.09 to create better performance for this targeted class of flows. With this in mind, Ray *et al* [24] used data from four cases of the transonic jet-in-crossflow experiment studied here, along with a Bayesian optimization, to determine refined values for the *k*-ε model coefficients that better aligned the primary vortex pair in the CFD results to that measured in the PIV. The improvement in the induced vortical velocity along the centerline of the interaction is evident in Fig. 2. This was made possible by use of a specific value for C_μ of 0.1025 rather than the broadly accepted 0.09. In a follow-up paper, Ray *et al* [25] applied the same calibration procedure to a wider range of experimental jet-in-crossflow data and again determined that a value of $C_\mu = 0.1025$ was appropriate for these flows.

Miller *et al* [26] examined the performance of the calibrated RANS model over a much larger parameter space. A total of 48 test cases from various Beresh *et al* publications were tested, involving a variety of jet interaction strengths, nozzle inclinations, and measurement stations. A flight vehicle configuration incorporating spin rockets was included as well. Figure 3 shows an example of the results, here for a metric of the mean-squared error of the simulation with respect to the PIV velocity field, which is essentially an overall picture of the agreement of the RANS computation and the PIV. Nearly every case shows a dramatic reduction in the error when using the optimal calibrated model (C_{opt}) as opposed to the nominal model (C_{nom}). Five additional metrics were considered in Miller *et al* and all but one showed similarly strong improvement.

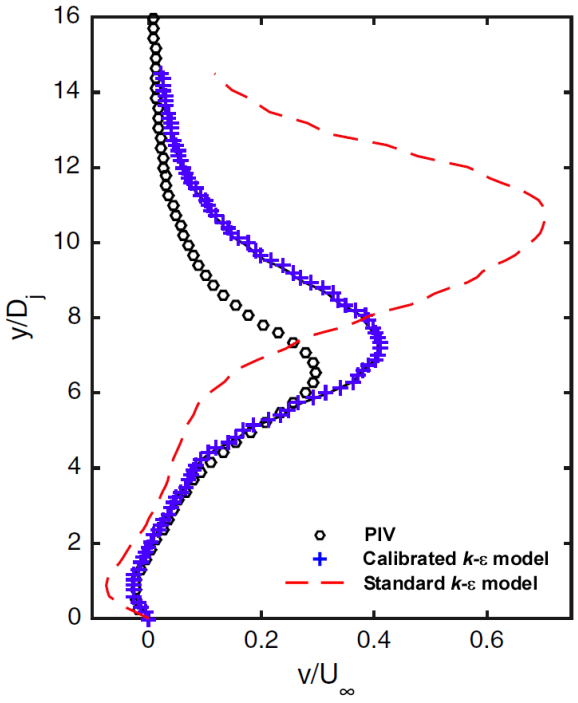

Fig. 2 Centerline velocity induced by the vortex pair in a jet-in-crossflow for a standard k-ε model with C_μ of 0.09, a calibrated k-ε model with C_μ of 0.1025, and the matching PIV data. Ray *et al* [24].

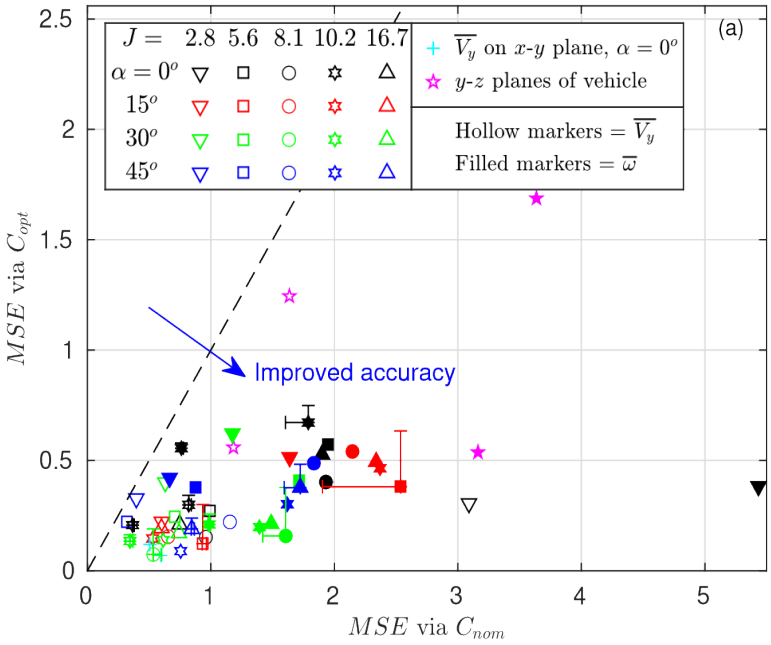

Fig. 3 Mean-square error (MSE) of 48 test cases compared to the PIV, with the standard k-ε model (C_{nom}) and the calibrated k-ε model (C_{opt}). Mean velocity and vorticity both are tested. Miller *et al* [26].

Remarkably, this recalibration of C_μ based on only four cases of a transverse jet yielded accuracy improvements in nearly every case among the 48. Even simulations of a flight vehicle configuration with substantial complexity beyond the canonical jet-in-crossflow improved markedly in its comparison to PIV data [27] (the pink five-pointed stars in the figure).

These efforts demonstrate that if a universal value for C_μ exists and is applicable for this jet-in-crossflow interaction, small changes in its value produce large variation in the behavior of the simulations, and that the resulting improvements are sufficiently robust to aid cases well beyond the canonical geometries from which it was calibrated. This indicates that a concerted effort to refine the value of C_μ may pay great dividends. The Ray *et al* approach to recalibrating C_μ merely uses the mean velocity field from PIV. But of course modern PIV techniques are capable of delivering much higher fidelity data, and therefore more sophisticated approaches may be considered.

4. Variable C_μ RANS Model

A more sophisticated approach to determining C_μ is possible using the spatial fidelity of PIV. If all the values in Eqns. (1) and (2) are available from the PIV, C_μ may be calculated directly from the PIV data. In this manner, C_μ can be optimized locally in a flow rather than just an optimal constant throughout the flow as in the calibrated model of Section 3.

The details of this approach are lengthy and provided in Miller and Beresh [23], but they are briefly described here. The stereoscopic planar PIV data provided all six unique components of the Reynolds stress tensor and thus all components of the anisotropy tensor (right side of Eq. 1). The data only provided three of the unique components of the mean rate-of-strain tensor (left side of Eq. 1) because out-of-plane gradients are not resolved by planar PIV. The absent terms could be approximated by leveraging the orthogonal data planes as shown in Fig. 1 and employing reasonable assumptions such as divergence-free flow and negligible out-of-plane gradients along the centerline. With all terms in Eq. (1) thusly present, the scalar eddy viscosity ν_t was found via a least-squares fit across all components of the tensors. It is shown in Fig. 4 on both *x*-*y* and *y*-*z* planes.

Direct calculation of C_μ also requires the determination of k and ε from the PIV data, as per Eq. (2). The turbulent kinetic energy k was readily available from the Reynolds stress data and its determination did not require any complex methods. It is given in Fig. 5. The dissipation rate ε was estimated using its relationship to Kolmogorov's similarity hypotheses and their application via the second-order longitudinal structure function [28]. These hypotheses can be simplified for application to a single axis in which the mean-square differences of velocities separated by a variable distance r along a coordinate axis are expected to vary as $r^{2/3}$ when r is within the inertial subrange. This relationship remains robust even when approaching the inertial subrange. Conveniently for present purposes, the scaling parameter is a known constant multiplied with the dissipation rate ε. This relationship has been exploited to calculate ε in a variety of applications (e.g. [29, 30]) and has been shown to be a stable and accurate way for estimating dissipation with stereoscopic PIV data [9]. The present ε fields are shown in Fig. 6.

At this point, a variable C_μ is now available at all spatial locations at which PIV data were acquired. However, simulation of an entire flow field requires C_μ at every point. To bridge this gap, a functional mapping between C_μ and the flow state variables is achieved using deep neural networks to train the algorithm via machine learning based on the available PIV data. The desired state variables that serve as model inputs are chosen from those identified by Pope [3] and include parameters such as mean strain rates and mean vorticity. The desired output is the three-dimensional field of C_μ, which then provides the Reynolds stresses needed to close the Reynolds-averaged conservation equations at any point in the simulation

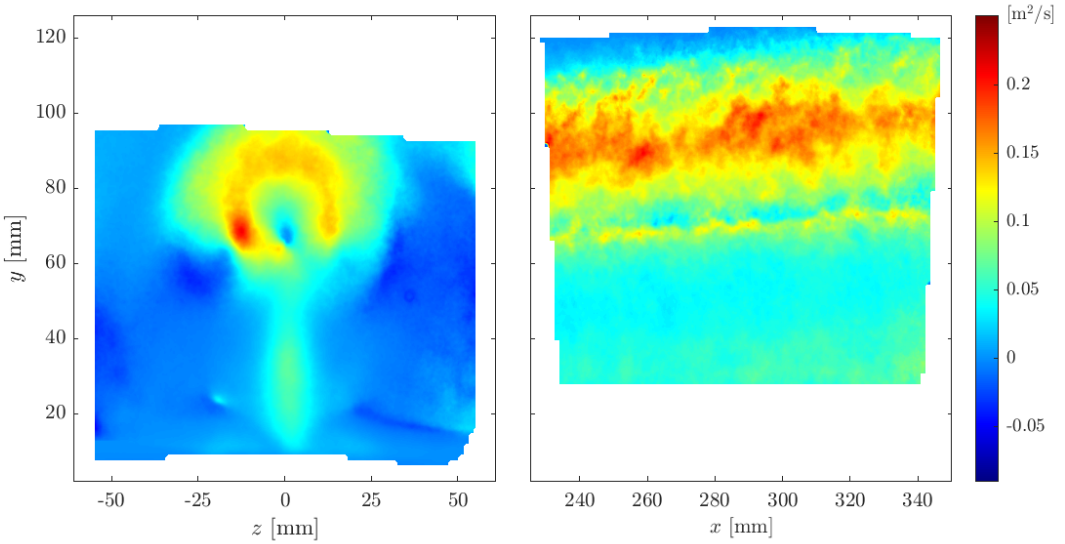

Fig. 4 The eddy viscosity ν_t calculated from PIV data; (a) y-z plane at x = 219 mm; (b) x-y plane at z=0.

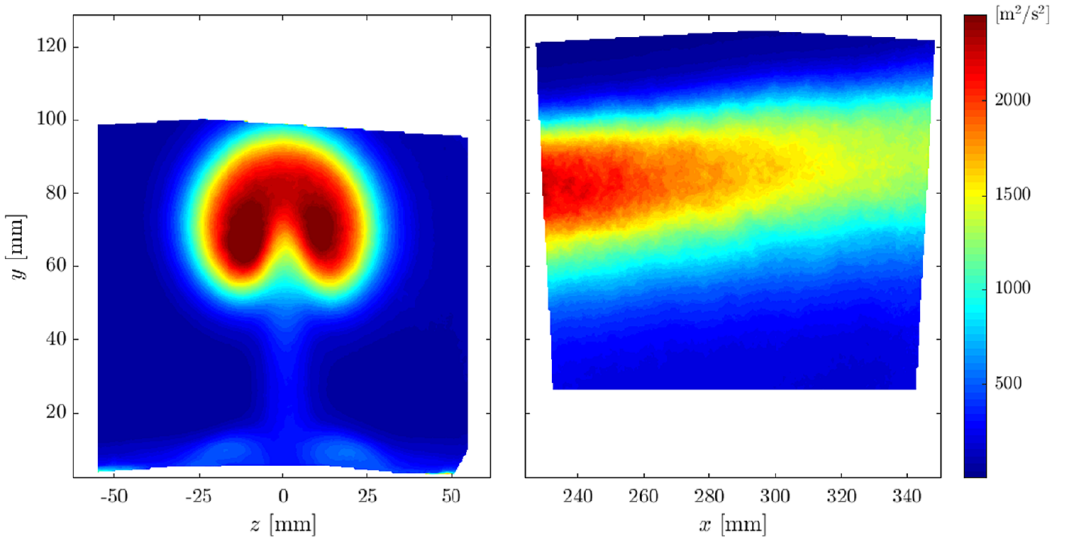

Fig. 5 The turbulent kinetic energy k calculated from PIV data; (a) y-z plane at x = 219 mm; (b) x-y plane at z=0.

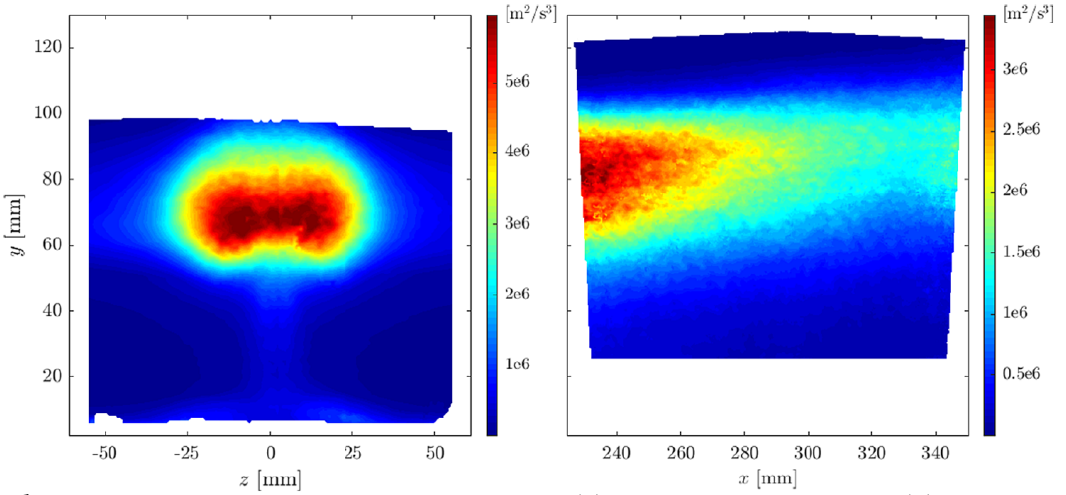

Fig. 6 The dissipation rate ε calculated from PIV data; (a) y-z plane at x = 219 mm; (b) x-y plane at z=0.

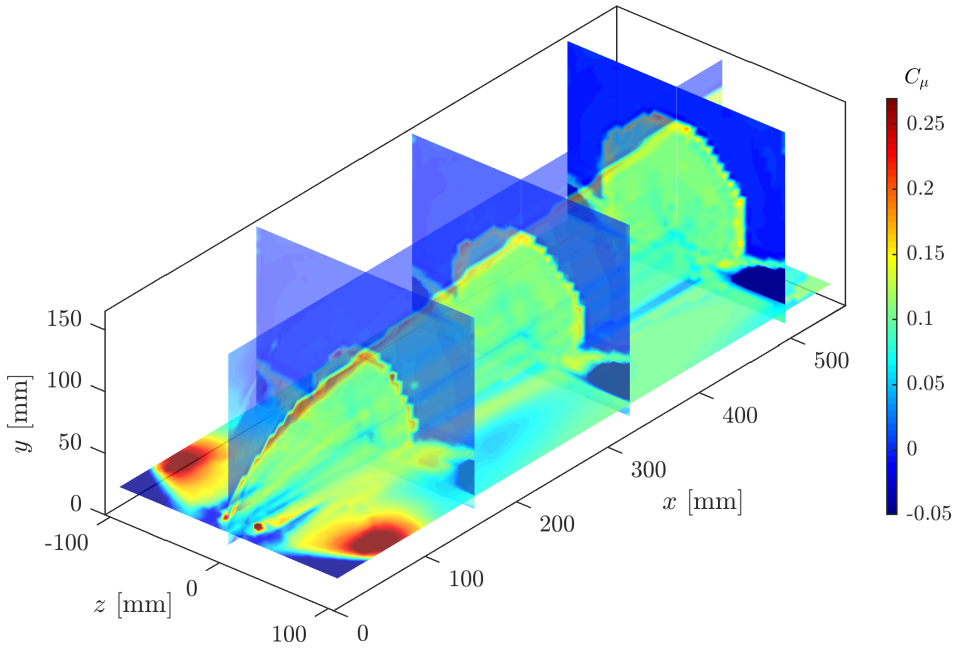

Fig. 7 Spatial mapping of the *k*-ε modeling parameter C_μ based on a machine-learned relationship to flow state variables trained from PIV data.

domain, not just those at PIV measurement locations. These state variables all are found in the PIV data and span across all test cases and spatial locations, freeing the mapping from dependance on any one particular flow condition. Once this mapping is complete, C_μ is obtainable over the entire computational domain, as shown in Fig. 7 for the case of a transverse jet. Other flow configurations are derived similarly by training to the same underlying PIV data sets but the resulting algorithm adapts to the local flow behavior such as to map C_μ to each flow topology. In this manner, a predictive capability may be generated that is generalized to jet interactions however they may be simulated rather than restricted to a single test case.

The process of determining an appropriate C_μ field for an individualized flow simulation must be incorporated into the RANS computational code itself. It is a substantial and specialized task to recraft a production *k*-ε simulation code to function with the present variable C_μ model, which is not described here. As this document is written, this task has been completed and verified and shown to yield a realistic jet-in-crossflow flow field, as seen in Fig. 8. However, early results demonstrate that the flow field simulated with the variable C_μ model is nearly identical to that produced by the original *k*-ε model without any C_μ modification, shown in Fig. 9. This disappointing result has been traced to three challenges.

The first challenge is that the PIV data comprises a limited portion of the simulation domain, and thus training data is not available for large portions of the domain containing important physics (e.g., the jet

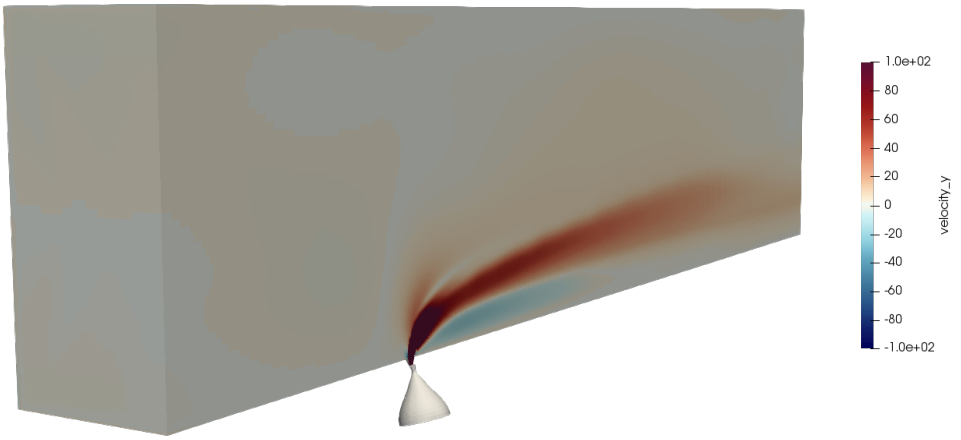

Fig. 8 Demonstration of the variable C_μ model for a k-ε RANS simulation on a jet-in-crossflow case.

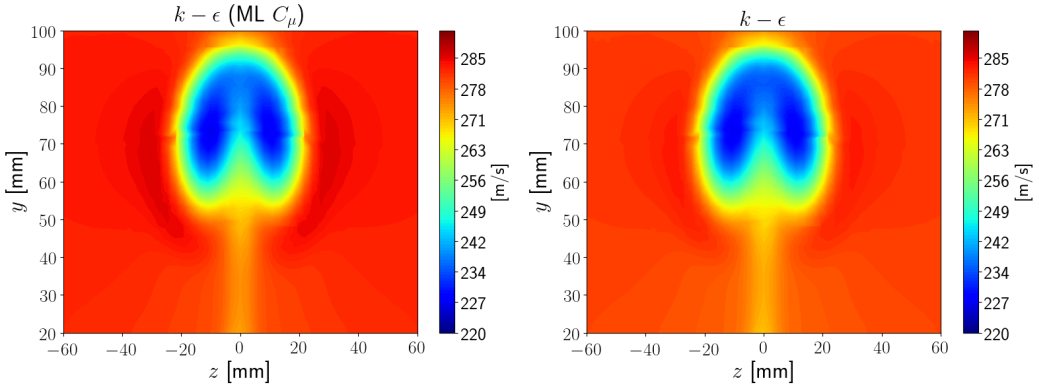

Fig. 9 Counter-rotating vortex pair at $\underline{x} = 219$ mm visualized via the streamwise velocity deficit; (left) variable C_μ model; (right) nominal k-ε model with canonical constant $C_\mu = 0.09$.

nozzle). In these locations C_μ cannot be found reliably from the data and a default C_μ is employed to avoid excessive model extrapolation in unmeasured regions or those in which the calculation "blows up" due to small values of one parameter or another. This default value, though predominantly in locations away from the core of the jet interaction, appears to wield a strong impact due to its prevalence throughout the computational domain. Preliminary results suggest that if the default C_μ is altered from the nominal value of 0.09 to the calibrated value of 0.1025 (section 3), the simulated flow field instead closely resembles the flow field predicted by the calibrated model. This supports the view that the choice of a default C_μ when a machine-learned value is unavailable tends to dominate the result.

The second challenge is that the data-driven model is designed to optimally predict an intrinsic model parameter (C_μ) as opposed to an extrinsic output quantity-of-interest (e.g., velocity fields). As a result, improved predictions for output quantities-of-interest rely on the assumption that the "truth" C_μ field computed from the PIV dataset will propagate through to improved quantity-of-interest predictions. This is in direct contrast to most calibration approaches such as the earlier calibrated C_μ that was directly tuned to optimally predict the counter-rotating vortex-pair.

The final challenge pertains to data consistency. In the present approach turbulent kinetic energy k and dissipation rate ε are used to non-dimensionalize input features to the data-driven model. It is well appreciated, however, that the k and ε fields predicted by RANS models differ significantly from their truth values. This inadequacy introduces a "data-inconsistency" to the formulation: the data-driven model is trained with "truth values" of k and ε as extracted from PIV, but then relies on RANS-generated values of these fields when deployed in the RANS code. This inconsistency can result in erroneous predictions of C_μ that limit the accuracy of the model (see Section 5.4 of [31]).

Novel techniques, including inverse modeling [32] and extrapolation detection [33, 34], are under development to address the above issues. These techniques directly couple training the data-driven model to the underlying RANS solver and aim to robustly classify extrapolation of the model. Thereby, more sensible choices of C_μ may be implemented beyond the limited bounds of the experimental data. Regardless, the preliminary results such as those displayed in Fig. 9 indicate that some additional digestion of the PIV data is required before it may be incorporated into an altered RANS model with improved predictive capacity.

However the spatially variable C_μ model evolves, it represents a blending of CFD with modern experimental techniques to craft a more successful predictive capability. This variable C_μ approach may be characterized as a data-driven turbulence model because the modeling constant C_μ has been reshaped as a spatially dependent variable determined by experimentally measured flow field properties. It also may be viewed as a data assimilation technique, but unlike those that have become common for volumetric TR-PIV measurements, it yields a generalized model capable of making flow predictions as in the ordinary application of RANS, as opposed to only serving the test case actually measured.

5. Conclusions and Future Work

The present effort seeks to improve the predictive capability of RANS models by incorporating PIV data through the use of deep learning in data-driven models. The key parameters in a k-ε turbulence model are the turbulent kinetic energy, the dissipation rate, and the eddy viscosity, all of which may be directly measured in a well-crafted PIV experiment. These flow field measurements allow determination of the modeling constant C_μ in a spatially varying manner rather than assuming it a universal constant as in a nominal k-ε model. This approach is anticipated to introduce improved physical fidelity into the RANS model for the class of flows that the training data represent, without requiring alteration to the existing RANS closure models or computational structure.

In a simple initial implementation, the nominal value of the model coefficient C_μ was replaced with an optimized value calibrated to the PIV results from only four flow cases of a configuration of a transverse jet exhausting from a flat plate at varied jet strength. Yet the optimized model demonstrated superior performance over 48 flow cases of increasing complexity, including a flight vehicle configuration substantially different from the canonical training data.

A second, more sophisticated data-driven model was created by mapping a spatially variable C_μ to flow state variables using machine learning of experimentally measured flow field properties of the turbulence. This permits local optimization of the model parameter rather than simply selecting an optimal constant throughout the flow field. This second model has been implemented in a production RANS code and has been shown to return physically plausible results, but these predictions closely match the results from either the nominal or calibrated C_μ models depending upon how values of C_μ are extrapolated beyond the core of the flow where PIV measurements are available. Continued development of the spatially variable C_μ model will incorporate more advanced deep learning techniques such as extrapolation detection and discrepancy models using a RANS feedback loop to more broadly estimate C_μ from the experimental training data. Then, in the same manner that the calibrated C_μ model was validated against a suite of 48 cases plus a flight vehicle configuration, the new variable C_μ model may be tested for its predictive capability of jet interactions. Whereas data assimilation techniques that have become common for volumetric TR-PIV measurements can improve the physical fidelity only of the test case actually measured, the approach under development here yields a generalized RANS model with improved physical fidelity that can be applied to predict any relevant flow case.

Acknowledgments

Sandia National Laboratories is a multi-mission laboratory managed and operated by National Technology and Engineering Solutions of Sandia, LLC., a wholly owned subsidiary of Honeywell International, Inc., for the U.S. Department of Energy's National Nuclear Security Administration under contract DE-NA0003525. This paper describes objective technical results and analysis. Any subjective views or opinions that might be expressed in the paper do not necessarily represent the views of the U.S. Department of Energy or the United States Government.

References

[1] Mahesh, K., "The Interaction of Jets with Crossflow," *Annual Review of Fluid Mechanics*, Vol. 45, 2013, pp. 379-407.

[2] Jones, W. P., and Launder, B. E., "The Prediction of Laminarization with a Two-Equation Model of Turbulence," *Int. J. Heat Mass Trans.*, Vol. 15, 1972, pp. 301–314.

[3] Pope, S. B., *Turbulent Flows*, Cambridge University Press, U. K., 2000.

[4] Craft, T. J., Launder, B. E., and Suga, K., "Development and Application of a Cubic Eddy-Viscosity Model of Turbulence,"

Int. J. of Heat and Fluid Flow, Vol. 17, 1996, pp. 108–115.

[5] Feng, H., Olsen, M. G., Hill, J. C., and Fox, R. O., "Simultaneous Velocity and Concentration Field Measurements of Passive-Scalar Mixing in a Confined Rectangular Jet," *Experiments in Fluids*, Vol. 42, No. 6, 2007, pp. 847-862.

[6] Shao, D., and Law, A. W.-K., "Turbulent Mass and Momentum Transport of a Circular Offset Dense Jet," *Journal of Turbulence*, Vol. 10, No. 40, 2009, pp. 1-24.

[7] Coletti, F., Benson, M. J., Ling, J., Elkins, C. J., and Eaton, J. K., "Turbulent Transport in an Inclined Jet in Crossflow," *Int. J. of Heat and Fluid Flow*, Vol. 43, 2013, pp. 149-160.

[8] Bai, K., Katz, J., and Meneveau, C., "Turbulent Flow Structure Inside a Canopy with Complex Multi-Scale Elements," *Boundary-Layer Meteorology*, Vol. 155, No. 3, 2015, pp. 435-457.

[9] de Jong, J., Cao, L., Woodward, S. H., Salazar, J. P. L. C., Collins, L. R., and Meng, H., "Dissipation Rate Estimation from PIV in Zero-Mean Isotropic Turbulence," *Experiments in Fluids*, Vol. 46, 2009, pp. 499–515.

[10] Xu, D., and Chen, J., "Accurate Estimate of Turbulent Dissipation Rate using PIV Data," *Experiments in Thermal and Fluid Science*, Vol. 44, 2013, pp. 662–672.

[11] Tanaka, T., and Eaton, J. K., "A Correction Method for Measuring Turbulence Kinetic Energy Dissipation Rate by PIV," *Experiments in Fluids*, Vol. 42, 2007, pp. 893–902.

[12] Zaripov, D., Li, R., and Dushin, N., "Dissipation Rate Estimation in the Turbulent Boundary Layer using High-Speed Planar Particle Image Velocimetry," *Experiments in Fluids*, Vol. 60, No. 1, 2019, p. 18.

[13] Schneiders, J. F. G., Dwight, R. P., and Scarano, F., "Time-Supersampling of 3D-PIV Measurements with Vortex-in-Cell Simulation," *Experiments in Fluids*, Vol. 55, No. 3, 2014, p. 1692.

[14] Schneiders, J. F. G., and Scarano, F., "Dense Velocity Reconstruction from Tomographic PTV with Material Derivatives," *Experiments in Fluids*, Vol. 57, No. 9, 2016, pp. 139.

[15] Jeon, Y. J., Schneiders, J. F. G., Müller, M., Michaelis, D., and Wieneke, B., "4D Flow Field Reconstruction from Particle Tracks by VIC+ with Additional Constraints and Multigrid Approximation," 18th International Symposium on Flow Visualization (Zurich, Switzerland), 2018.

[16] Gesemann, S., Huhn, F., Schanz, D., and Schröder, A., "From Noisy Particle Tracks to Velocity, Acceleration and Pressure Fields using B-splines and Penalties," *18th International Symposium on Applications of Laser Techniques to Fluid Mechanics (Lisbon, Portugal)*, 2016.

[17] Ehlers, F., Schröder, A., and Gesemann, S., "Enforcing Temporal Consistency in Physically Cconstrained Flow Field Reconstruction with FlowFit by Use of Virtual Tracer Particles," *Measurement Science and Technology*, Vol. 31, No. 9, 2018, pp. 094013.

[18] Beresh, S. J., Henfling, J. F., Erven, R. J., and Spillers, R. W., "Penetration of a Transverse Supersonic Jet into a Subsonic Compressible Crossflow," *AIAA Journal*, Vol. 43, No. 2, 2005, pp. 379–389.

[19] Beresh, S. J., Henfling, J. F., Erven, R. J., and Spillers, R. W., "Crossplane Velocimetry of a Transverse Supersonic Jet in a Transonic Crossflow," *AIAA Journal*, Vol. 44, No. 12, 2006, pp. 3051–3061.

[20] Beresh, S. J., Wagner, J. L., Henfling, J. F., Spillers, R. W., and Pruett, B. O. M., "Comparison of Pulse-Burst PIV Data to Simultaneous Conventional PIV Data," *AIAA Paper 2016-0789*, 2016.

[21] Beresh, S. J., Henfling, J. F., Spillers, R. W., and Pruett, B., "Influence of the Fluctuating Velocity Field on the Surface Pressures in a Jet/Fin Interaction," *J. Spacecraft Rockets*, Vol. 55, No. 5, 2018, pp. 1098–1110.

[22] Beresh, S. J., Miller, N. E., and Smith, B. L., "Practical Challenges in the Calculation of Turbulent Viscosity from PIV Data," AIAA Paper 2018-2987, 2018.

[23] Miller, N. E., and Beresh, S. J., "Using Particle Image Velocimetry to Determine Turbulence Model Parameters," *AIAA Journal*, Vol. 59, No. 3, 2021, pp. 842-854.

[24] Ray, J., Lefantzi, S., Arunajatesan, S., and Dechant, L., "Bayesian Parameter Estimation of a k–ε Model for Accurate Jet-in-Crossflow Simulations," *AIAA Journal*, Vol. 54, No. 8, 2016, pp. 2432–2448.

[25] Ray, J., Dechant, L., Lefantzi, S., Ling, J., and Arunajatesan, S., "Robust Bayesian Calibration of a k–ε Model for Compressible Jet-in-Crossflow Simulations," *AIAA Journal*, Vol. 56, No. 12, 2018, pp. 4893–4909.

[26] Miller, N. E., Beresh, S. J., and Ray, J., "Validation of Calibrated k-ε Model Parameters for Jet-in-Crossflow," accepted for publication in *AIAA Journal*, published online at https://doi.org/10.2514/1.J061396.

[27] Beresh, S. J., Heineck, J. T.,Walker, S. M., Schairer, E. T., and Yaste, D. M., "Planar Velocimetry of Jet/Fin Interaction on a Full-Scale Flight Vehicle Configuration," *AIAA Journal*, Vol. 45, No. 8, 2007, pp. 1827–1840.

[28] Monin, A. S., and Yaglom, A. M., *Statistical Fluid Mechanics: Mechanics of Turbulence Volume II*, The MIT Press, Cambridge, Mass., 1975.

[29] Wiles, P. J., Rippeth, T. P., Simpson, J. H., and Hendricks, P. J., "A Novel Technique for Measuring the Rate of Turbulent Dissipation in the Marine Environment," *Geophys. Res. Letters*, Vol. 33, 2006.

[30] Miller, N. E., Stoll, R., Mahaffee, W. F., and Pardyjak, E. R., "Mean and Turbulent Flow Statistics in a Trellised Agricultural Canopy," *Boundary-Layer Meteorology*, Vol. 165, 2017, pp. 113–143.

[31] Duraisamy, K., Iaccarino, G., and Heng, X., "Turbulence Modeling in the Age of Data", *Annual Review of Fluid Mechanics*, Vol. 51, 2019, pp. 357-377.

[32] Duraisamy, K., Zhang, Z. J., and Singh, A. P., "New Approaches in Turbulence and Transition Modeling Using Data-driven Techniques", AIAA Paper 2015-1284, 2015.

[33] Barone, M., Ray, J., and Domino, S., "Feature Selection, Clustering, and Prototype Placement for Turbulence Datasets," *AIAA Journal*, Vol. 60, No. 3, 2022, pp. 1332-1346.

[34] Rumsey, C. L., Coleman, G. N., and Wang, L., "In Search of Data-Driven Improvements to RANS Models Applied to Separated Flows," AIAA Paper 2022-0937, 2022.